JOURNAL OF MATERIALS SCIENCE 28 (1993) 3027–3034

Micromechanisms of compressive failure in a glass fibre-reinforced amorphous thermoplastic

J. LANKFORD
Materials and Mechanics Department, Southwest Research Institute, San Antonio, TX 78228, USA

Compressive failure of a 0°/90° glass fibre-reinforced amorphous thermoplastic has been characterized. It was found that the critical event is the nucleation within 90° laminates of multiple shear crazes, which become shear microcracks, transition to axial cracks, and permit the specimen to fail by the flexure of 0° elements. It is shown that the apparent kinetics of this process provide a rationale for the dramatic strain-rate strengthening of these composites at high loading rate.

1. Introduction

In a recent study [1], the compressive behaviour of a unidirectional PAN-derived carbon fibre-reinforced semicrystalline thermoplastic was characterized. Results obtained contrasted with those associated with earlier work [2, 3] involving thermoset–matrix composites. It was found, for example, that the thermoplastic-based composites yield well below failure, and that the latter occurs, with no precursory acoustic emission, via the sudden nucleation and propagation across the specimen of an unstable kink shear band. Further, it was determined that at high loading rates, the kinetics of kink propagation appeared to be responsible for a dramatic increase in strength, i.e. strain-rate hardening. Finally, it was noted that the matrix accommodated the formation of kinks by local yielding; the matrix itself did not fail by microfracture or microvoid formation until late in the development of a macroscopic shear band.

On-going work has as its objective the assessment of the influence of composite composition and architecture on the compressive failure process. To that end, the present paper reports the compressive behaviour of an amorphous thermoplastic reinforced with glass fibres laid up in 0°/90° laminates. It will be seen that the results offer both similarities and contrasts with regard to the preceding findings.

2. Material

The particular composite chosen for study was an amorphous polyimide copolymer (J-2, E.I. DuPont De Nemours, Inc., Wilmington, DE) reinforced with 15 μm diameter E-glass fibres. A polyetheretherketone (PEEK) derivative, the matrix has a low density (1.15 $g\,cm^{-3}$) and a melt laminate processing temperature of approximately 300 °C [4]. Unidirectional laminates of thickness of the order of 150 μm were laid up in a 0°/90° arrangement; laminates were composed of 60 vol % fibres. The elastic modulus for the fibres was 75 GPa [5], while that of the matrix was only 3.2 GPa [4]. The final void content of the composites was less than 1%.

3. Experimental procedure

Design and verification of the compression test configuration has been detailed elsewhere (Fig. 1). In particular, it was shown [1] that the cylindrically symmetric design (required for testing in a split Hopkinson pressure bar apparatus) yields quasistatic compressive strengths and evinces failure mechanisms essentially identical to those obtained in standard flat panel specimen configurations [6, 7]. The internally chamfered rings around the bases of the specimen were made of high-strength steel, honed to a snug fit. All specimens, as well as matching hardened steel load platens, were carefully machined so that mating surfaces were parallel within 4 μm over the load surface diameter.

Using a standard servo-controlled hydraulic machine, compression experiments were performed at strain rates, $\dot{\varepsilon}$, ranging from 5×10^{-6}–$5\,s^{-1}$. For $\dot{\varepsilon} \leqslant 10^{-4}\,s^{-1}$, acoustic emission (AE) was monitored using a transducer resonant at 160 kHz, with a filter-limited range of 100 kHz–1 MHz. Earlier work [8, 9] has shown that this frequency regime corresponds to that of stress-wave emission for microfracture in brittle materials such as ceramics.

Higher strain rates were achieved using the split Hopkinson pressure bar (SHPB) apparatus alluded to earlier. In particular, the latter experiments corresponded to $10^{3}\,s^{-1} \leqslant \dot{\varepsilon} < 10^{4}\,s^{-1}$. Generally, such tests result in total failure of the sample; however, by reducing the incident projectile velocity slightly, it was possible to damage, without failing, some of the specimens.

These, and other samples loaded quasistatically to various damage levels, were sectioned and examined by optical and scanning electron microscopy (SEM).

0022–2461

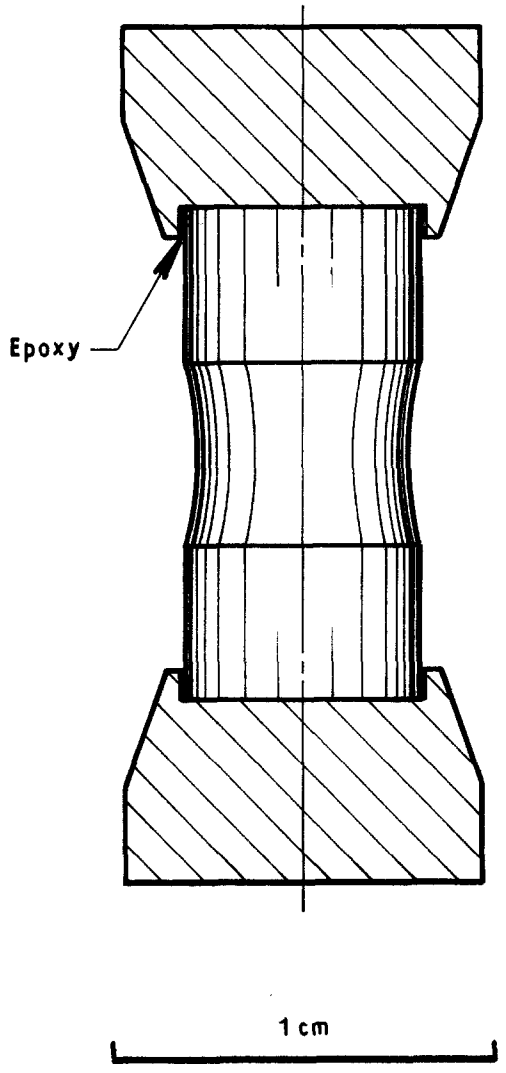

Figure 1 Configuration of compression test specimen.

Specimens for SEM study were vapour-deposited with gold, and imaged at low accelerating voltage to preclude electron-beam damage of the polymeric component.

4. Results

Fig. 2 shows a typical stress-strain, σ–ε, curve generated at a strain rate of $6 \times 10^{-6}\,s^{-1}$. Such results were obtained for all tests performed in the hydraulic machine, while the SHPB is incapable of discriminating the gradual, low-level yielding shown in the figure; thus the latter test provided ultimate stress data only.

Also plotted in Fig. 2 is the cumulative acoustic emission associated with damage development in the composite. It is evident that the threshold stress level for acoustic emission, σ_{AE}, is considerably in excess of the yield strength, σ_y. On the other hand, σ_{AE} is well below the ultimate strength, σ_C, indicating that the failure process is non-catastrophic, and probably requires the attainment of some critical state of damage.

Data for all specimens tested are summarized in Fig. 3. For strain rates below about $100\,s^{-1}$, ultimate strength increases gradually with strain rate, a trend which is parallelled by that of σ_y and σ_{AE}. However, for $\dot{\varepsilon} > 100\,s^{-1}$, there ensues a rapid increase in σ_c with $\dot{\varepsilon}$; analysis of the latter results shows that within this regime, $\sigma_C \propto \dot{\varepsilon}$.

Specimens tested under quasistatic conditions to the point of failure are characterized by the formation of a major shear plane, preceded by axial splitting, as shown in Fig. 4. Closer inspection (Fig. 5) shows that the splitting is isolated within the 90° laminates, and proceeds by growing around the periphery of near-

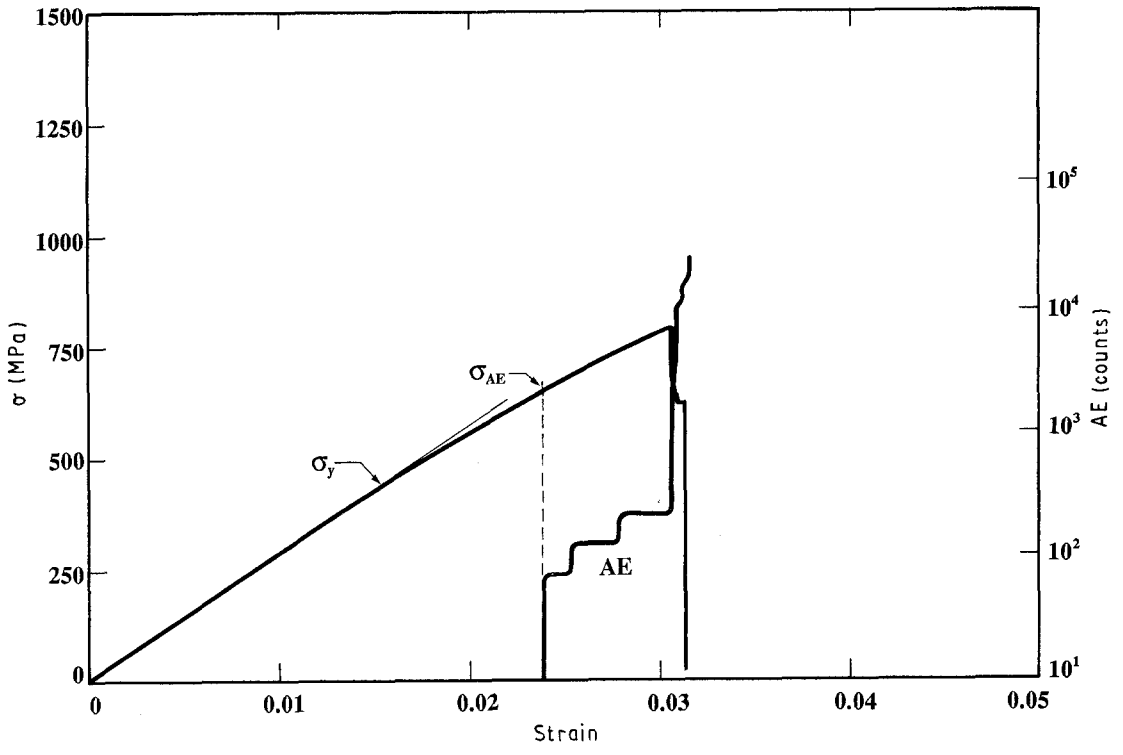

Figure 2 Compressive stress and acoustic emission versus strain, $\dot{\varepsilon} = 6 \times 10^{-6}\,s^{-1}$.

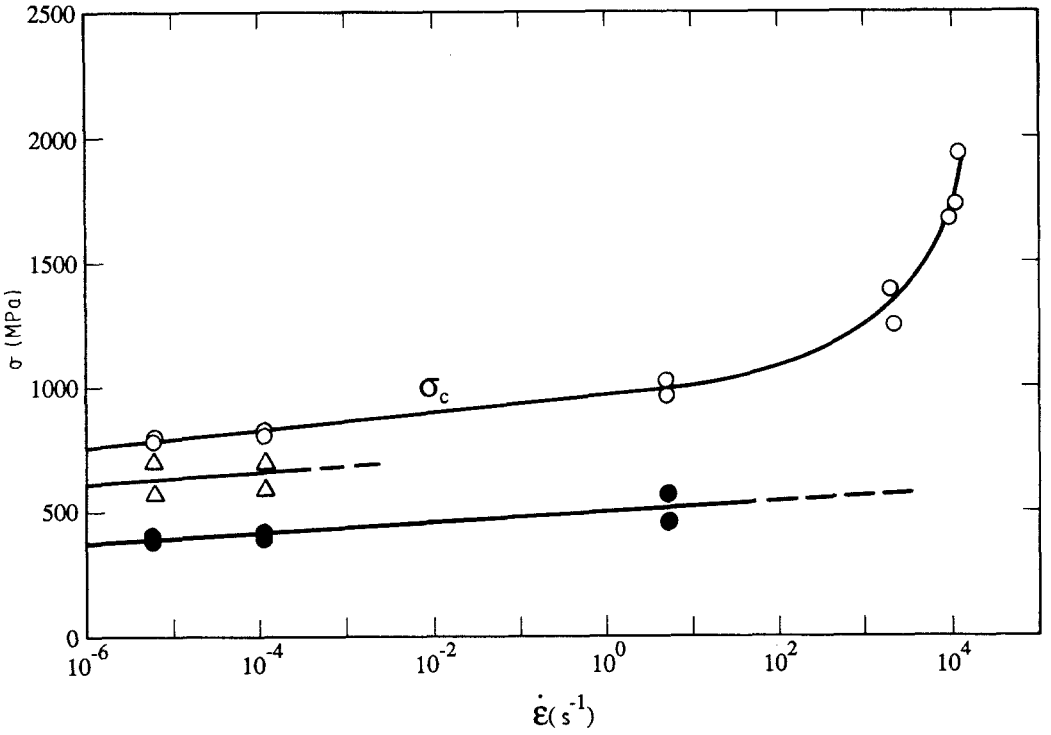

Figure 3 Stress level versus strain rate.

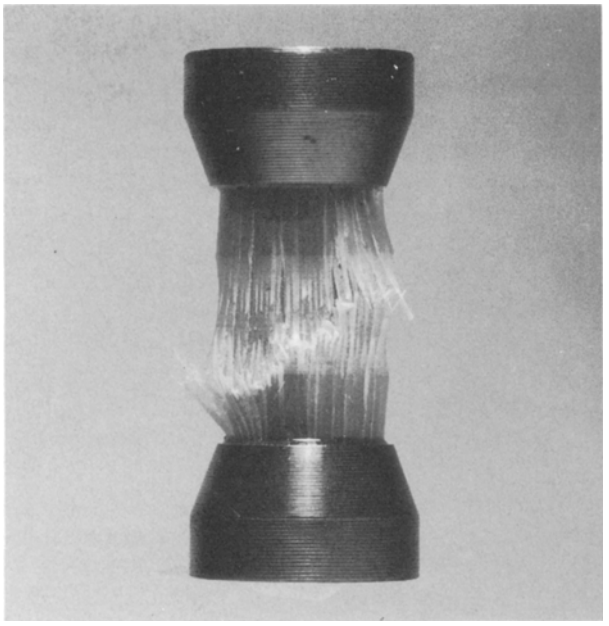

Figure 4 Macroscopic view of failed specimen, $\dot{\varepsilon} = 1 \times 10^{-4}\ s^{-1}$, showing shear failure preceded by axial splitting.

adjoining glass fibres and through the intervening matrix.

Although these macroscopic cracks are axially oriented, their early stages of development are dominated by shear. In particular, they seem to nucleate near 90° fibre–matrix interfaces (Fig. 6a), and apparently correspond to the breakdown of craze zones (Fig. 6b). Clusters of these craze zones eventually link (Fig. 7) to form an embryonic macrocrack, whose subsequent growth is axial. While the fibre–matrix interface is a critical factor in crack initiation, it is clear that the fibre–matrix bond strength is appreciable; one notes failed matrix microligaments adhering to the fibres in Fig 6b and 7.

Failure under more rapid loading conditions takes place according to a modification of this scenario. In particular, it can be seen (Fig. 8) that if a high strain-rate test is interrupted just prior to failure, the specimen will be characterized by an arrested "wave" of longitudinal splitting. In the figure, an untested specimen (left) is so oriented that the 0°/90° interfaces are parallel to the line of sight. After experiencing a dynamic load pulse, a similar specimen (right) has delaminated over nearly half its volume, the damage moving from left to right; apparently failure by macroscopic shear faulting does not occur until this sequential delamination process is complete. Closer inspection shows that the delamination process again occurs as for the quasistatic situation, i.e. with the 90° layers, with cracks running around the 90° fibre and across the matrix sectors which separate them. It should be noted that over the entire strain-rate regime, delamination is somewhat of a misnomer. In point of fact, the 0° and 90° lamellae never fail at their original interfaces. Instead, cracking within the 90° components creates sheets consisting of 0° zones sandwiched between 90° surface layers.

Again, as for lower strain rates, dynamic crack nucleation is shear dominated. Fig. 9 shows a region to the right of the arrested delamination wave of Fig. 8; this precursory damage is oriented at roughly 45° to the load axis, and associated with fibre–matrix fracture and matrix shear crackling. One of the shear cracks has arrested (arrow, Fig. 9) at a 0° fibre interface. Extensive study of 0° fibre bundles showed no intrinsic precursory damage or penetration by shear bands originating from 90° laminates.

At higher magnification (Fig. 10a), the structure of the arrested shear crack is seen to be derived from an

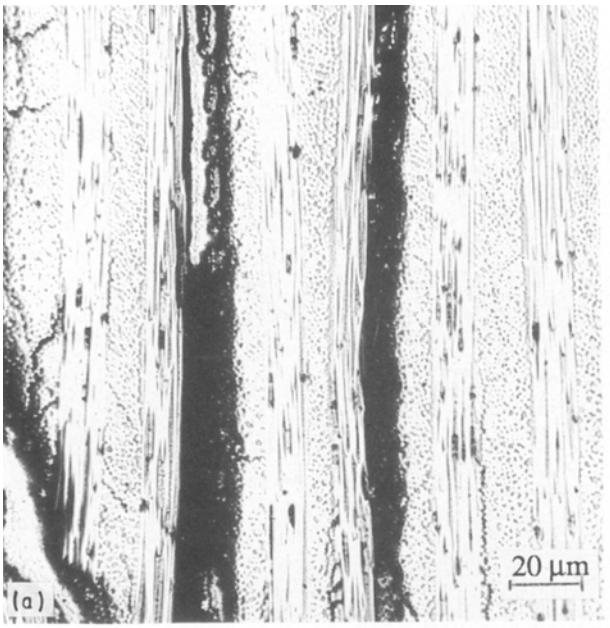

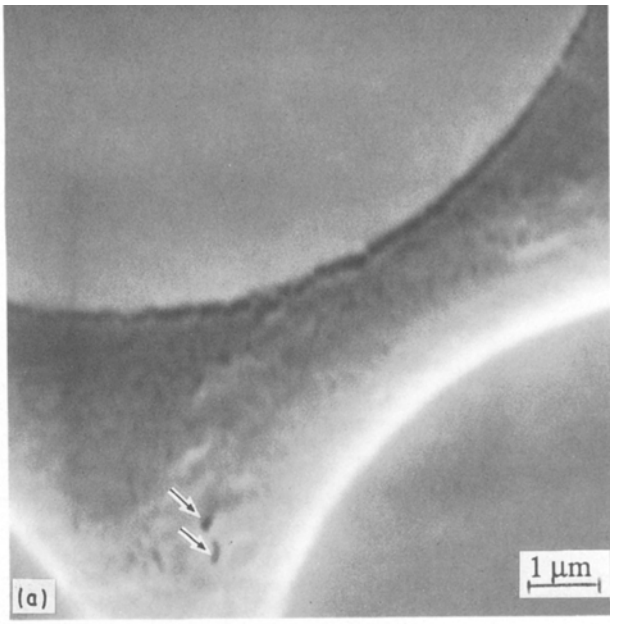

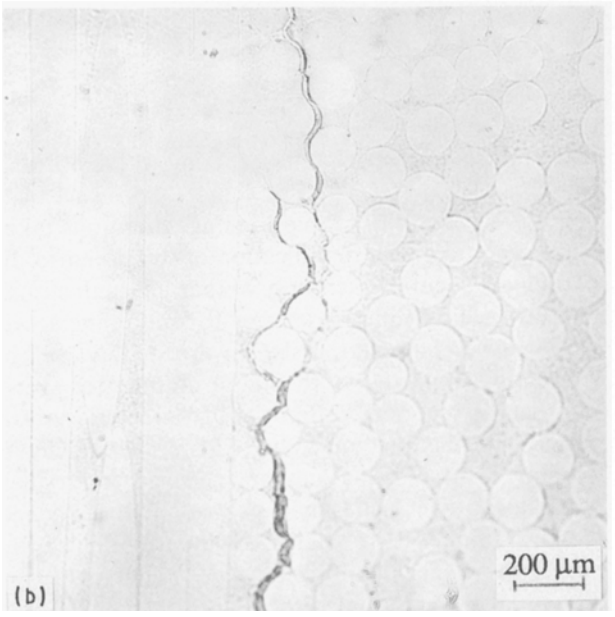

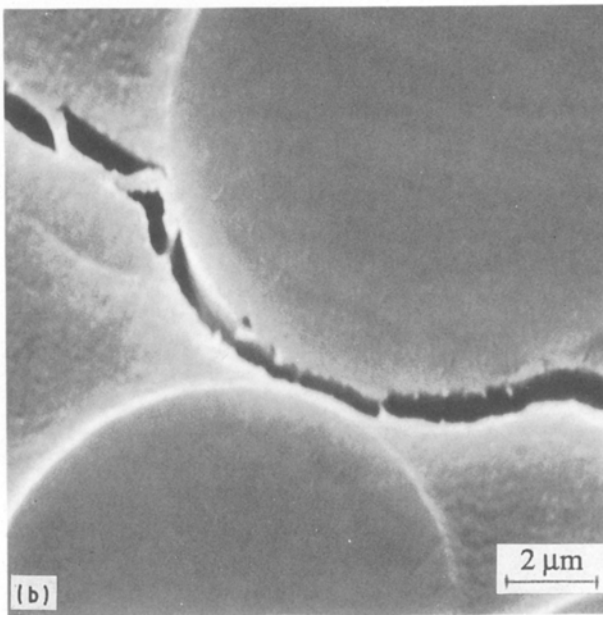

Figure 5 Axial damage development; $\dot{\varepsilon} = 1 \times 10^{-4}\ s^{-1}$, stress axis vertical, $\sigma = \sigma_C$. (a) Axial splitting, (b) axial crack development within 90° laminates.

Figure 6 Microcrack nucleation within 90° laminate; $\dot{\varepsilon} = 1 \times 10^{-4}\ s^{-1}$, stress axis vertical, $\sigma \simeq 0.95\sigma_C$. (a) Microcrack initiation near fibre interface; void formation (arrows) within apparent matrix shear band. (b) Transition of near-interface microcrack to shear-oriented craze crack.

initial shear craze. Breakdown of the craze generally does not occur within the midplane, but rather at locations (arrows, Fig. 10b) near the craze surface (i.e. the boundary with the parent matrix). In these photomicrographs, the structures shown represent local shear combined with Mode I (tensile) opening despite a nominal (vertical axis) pure compressive field. Clearly the latter is modified by the local response of the composite constituents.

The earliest observable (via SEM) stages of damage, i.e. located as far as possible to the right of, hence preceding, the arrested delamination "wave" in Fig. 8, are shown in Fig. 11. In this case, a shear craze has formed near a 90° fibre situated just outside the field of view in the lower right corner. The craze has grown toward the upper right, and has stopped just short of the 0° fibre at the left of the photo. Craze breakdown by a process of hole nucleation and coalescence has begun; the holes tend to nucleate near the craze surface, and by linking up will eventually produce the morphology shown in Fig. 10.

5. Discussion

The foregoing observations raise several issues, which will be considered in the following section. In particular, these include (1) the sequence of events leading to failure versus that shown earlier to be responsible for the failure of unidirectional graphite fibre-reinforced semi-crystalline PEEK, and (2) how this sequence might relate to the enhanced sensitivity of strength to strain rate under dynamic loading conditions.

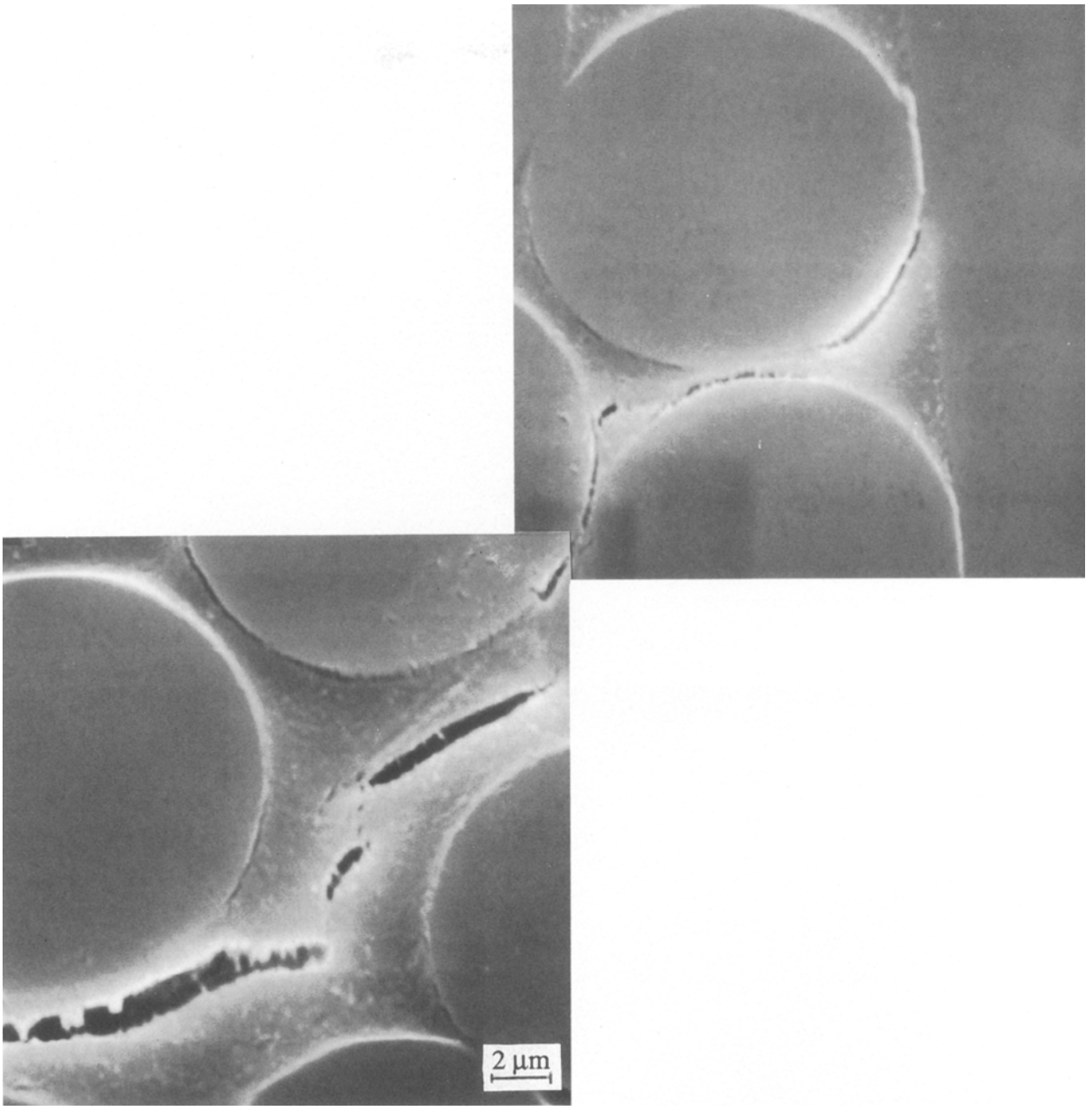

Figure 7 Linkup of shear microcracks within 90° laminate; $\dot{\varepsilon} = 1 \times 10^{-4}\,s^{-1}$, stress axis vertical, $\sigma \simeq 0.95\sigma_c$.

Clearly, the critical event in the failure of these composites lies in the nucleation of shear microcrazes within the 90° laminates. This seems to occur (Figs 6 and 7) very close to certain fibre–matrix interfaces, suggesting that it is the stress gradient or enhancement at a strongly bonded interface which is responsible. Because subsequent craze growth takes place within shear planes, it appears that both shear and local tension (to drive the opening of the craze surfaces and induce fibril drawing) must exist within certain enclaves of interacting 90° fibres, despite the nominal global compressive stress field. Finite element analysis probably will be required to characterize such enclaves. At this point, however, it seems reasonable to associate σ_y with near-interface matrix yielding by crazing.

Breakdown of microcrazes to form shear microcracks probably begins at slightly higher stresses, but still below σ_{AE}. Because this process seems to be one involving void nucleation rather than microfracture, it would not be expected to generate stress-wave emission.

This may not be true for the later stages of craze breakdown; however, Lauterwasser and Kramer [10] have performed detailed studies of the (micro) fracture of crazes in thick sheets of polystyrene (PS) loaded in pure tension. In these experiments, it was found that once a mature craze has formed, it will start to fail by slowly growing an embryonic crack along its midrib, a highly drawn fibrillar (hence lower density) region running along the central plane of the craze. Quickly, however, the imposition of the stress field of the embedded crack begins to generate highly drawn craze fibrils very close to the craze surface, i.e. further drawing of the midrib is not observed. This preferential strain localization eventually creates a situation in

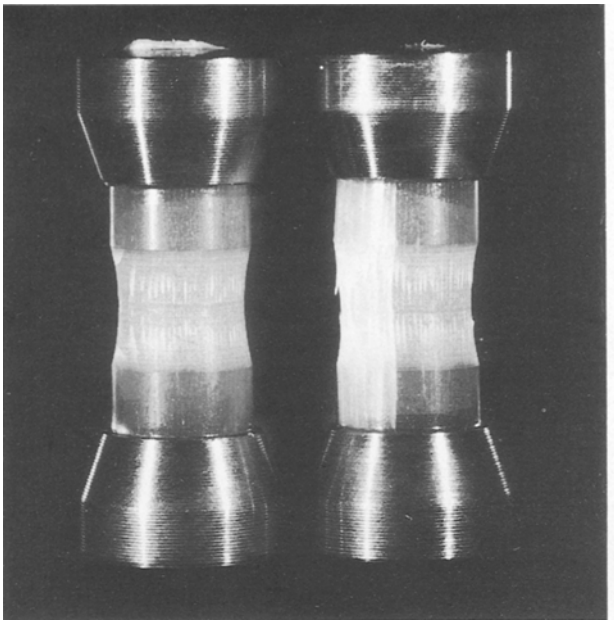

Figure 8 Untested specimen (left) versus sample (right) tested at $\dot{\varepsilon} = 4000\ s^{-1}$ to a near failure stress level ($\sigma \simeq 1500$ MPa).

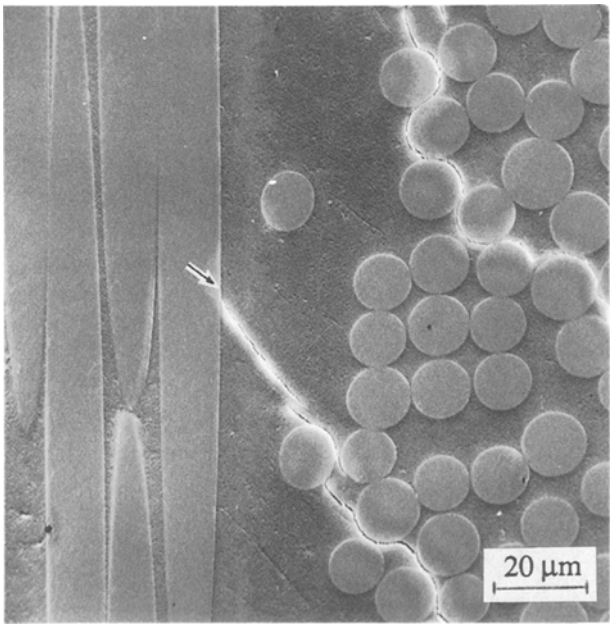

Figure 9 Dynamic shear crack nucleated in 90° laminate at $\dot{\varepsilon} \simeq 4000\ s^{-1}$, $\sigma \simeq 0.92\sigma_C$, compressive axis vertical; crack has arrested (arrow) at 0° fibre interface.

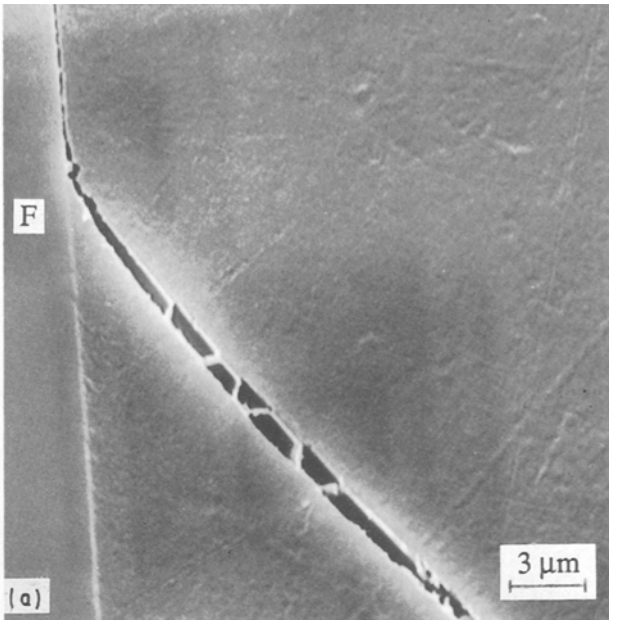

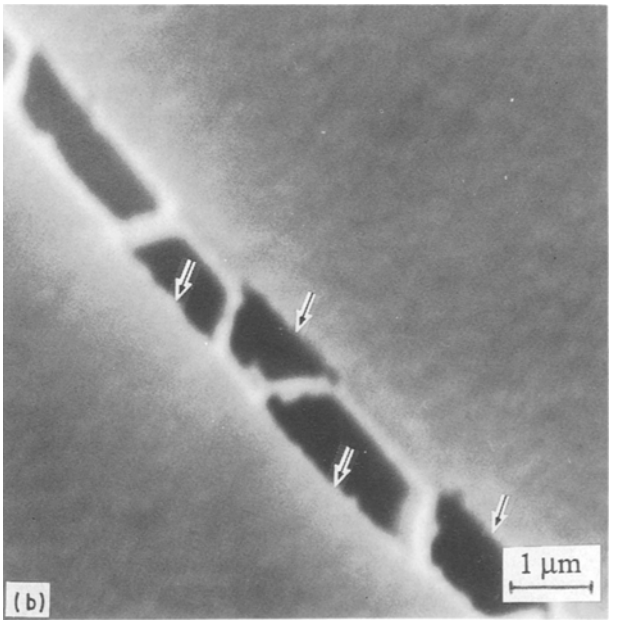

Figure 10 Details of shear band shown in Fig. 9. (a) Craze basis of shear band; craze arrest at 0° fibre interface (F). (b) Evidence of craze breakdown at craze surface (arrowed).

which, in the view of Lauterwasser and Kramer, it is essentially more favorable for the crack to advance through the highly drawn new craze zone at the craze/solid boundary than to continue to grow along the midrib. The result is rapid material separation alternating from one surface of the craze to the other, as observed in the present study for both quasistatic (Fig. 6b) and dynamic (Fig. 10) loading rates. Because this type of failure is caused by rapid increments in crack extension, it may generate acoustic emission, and hence could correspond to the global attainment of σ_{AE}.

Once a macroscopic crack has formed from the coalescence of a series of shear microcracks, there is a transition from shear to axial growth. This phase is probably facilitated by the tendency of hard fibres compressing relatively thin intervening matrix zones, to produce local tensile stresses normal to the compressive stress axis. Such stresses permit axial cracks to jump rapidly from one fibre to another, probably with significant acoustic emission. Under quasistatic conditions, this process may promote concurrent axial delamination throughout the specimen, while under dynamic loading, delamination once begun at a preferential near surface site proceeds across the sample in a fast wave. The speed of this wave will be controlled by craze nucleation/propagation kinetics.

At the point of basically complete delamination, the specimen still has not failed. Failure is reached shortly afterwards, as delaminated layers flex outwards, testing the tensile flaw distributions of the outermost

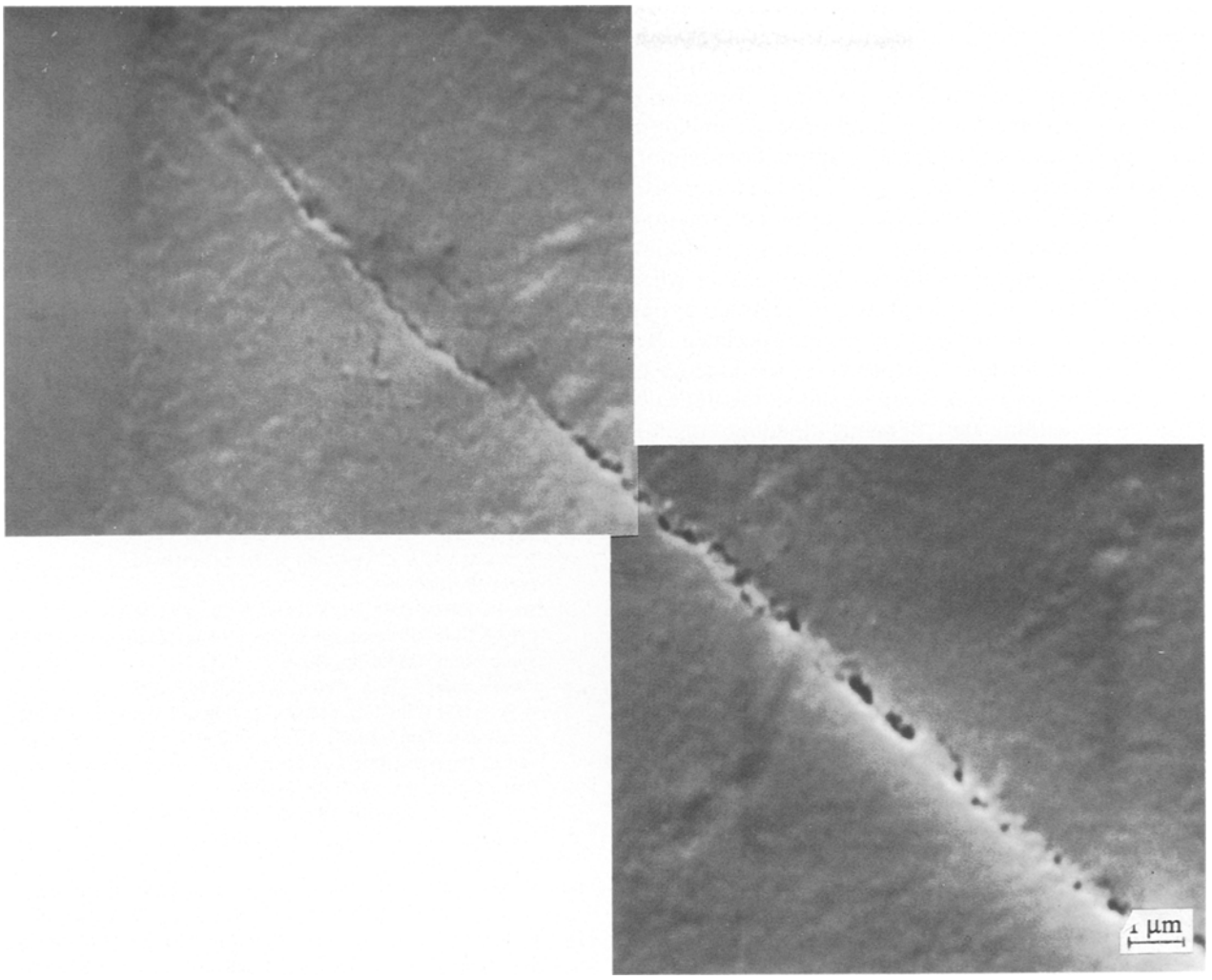

Figure 11 High-magnification view of early stages of craze breakdown via void nucleation to form shear crack; $\dot{\varepsilon} \simeq 4000\ s^{-1}$, $\sigma \simeq 0.92\sigma_C$; compressive axis vertical.

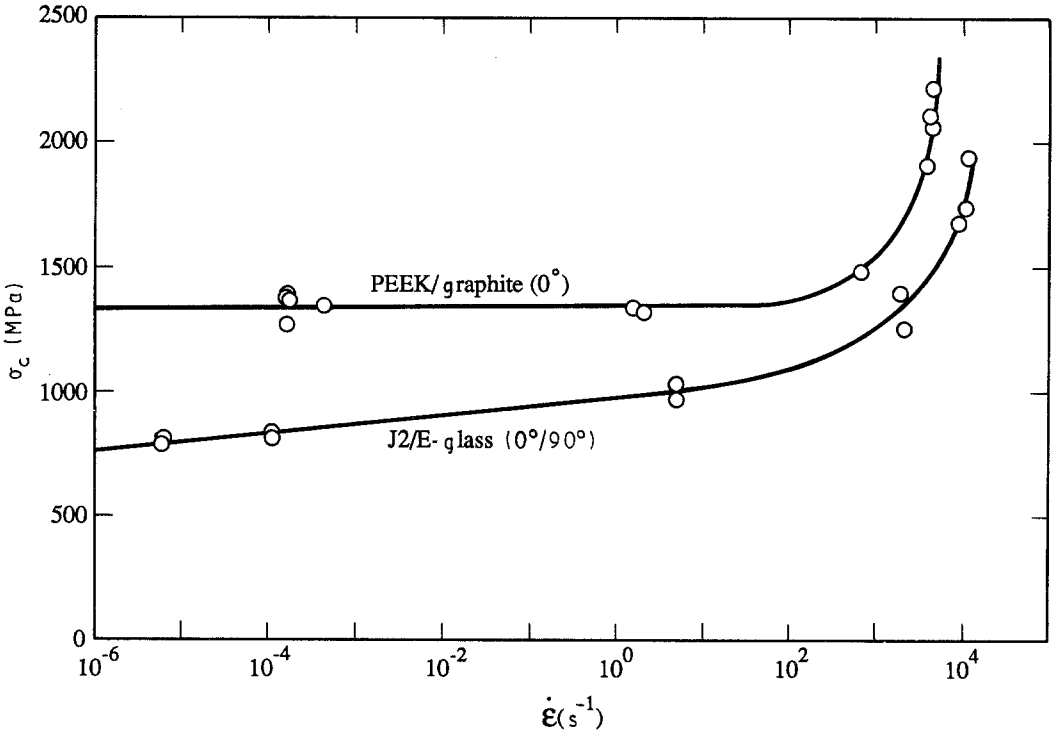

Figure 12 Compressive strength versus strain rate for unidirectionally graphite fibre-reinforced semicrystalline PEEK versus 0°/90° glass fibre-reinforced amorphous thermoplastic.

glass fibres [11]. These finally fail in bending (local tension), transferring the load to the next layer; subsequent gross failure is essentially instantaneous.

Interestingly, the strength–strain-rate dependence found for dynamic loading conditions is similar to that obtained earlier [1] for 0° graphite fibre-reinforced semicrystalline PEEK (Fig. 12). In the latter case, failure is initiated by classic matrix deformation, which at certain sites permits the nucleation of kink bands within individual fibres. Failure ensues when several of these kink bands grow and intersect, or one of them grows all the way across the specimen. Because the time for failure depends on the kinetics of shear band propagation, it can be shown theoretically [12] that within the dynamic loading regime, $\sigma_C \propto \dot{\varepsilon}^{1.0}$, a conclusion which was validated by the earlier experimental results.

In the present case, it is known [11] that E-glass fibres do not kink, but instead fail by the nucleation of tensile microcracks as the fibres flex. Thus, failure kinetics can be considered in terms of the following expression for the time to fail, i.e.

$$t_f = \frac{l_1}{C_1} + \frac{Nl_2}{C_2} \quad (1)$$

where l_1 is the distance that a shear crack within a 90° laminate must grow at a shear velocity C_1 before transitioning to an axial crack, and l_2 is the distance that N of these axial cracks must grow at a velocity C_2 before flex/failure can occur. Because the strain rate at failure can be written

$$\dot{\varepsilon} = \frac{\sigma_f}{Et_f} \quad (2)$$

where σ_f is the stress at failure and E the elastic modulus, substituting Equation 1 for t_f in Equation 2 yields

$$\sigma_f = E\left(\frac{l_1}{C_1} + \frac{Nl_2}{C_2}\right)^{-1}\dot{\varepsilon} \quad (3)$$

or $\sigma_f \propto \dot{\varepsilon}^{1.0}$. Thus, the same functional relationship is obtained as that established for the kink-prone unidirectional composite [1], but derived from a different physical process.

Acknowledgements

The meticulous experimental work of A. Nicholls is acknowledged with appreciation. Support of the Office of Naval Research through contract no. N00014-84-C-0213 is gratefully acknowledged.

References

1. J. LANKFORD, in "Advanced Composite Materials", edited by M. D. Sacks (American Ceramic Society, Westerville, OH, 1991) pp. 553–63.
2. C. CAZENEUVE and J. -C. MAILE, *J. Physique* **46** (1985) 551.
3. P. KUMAR, A. GARG and B. D. AGARWAL, *J. Aero. Soc. India* **38** (1986) 11.
4. W. H. KRUEGER, S. KHAN, R. B. CROMAN and I. Y. CHANG, in "Proceedings of the 33rd International SAMPE Symposium" (1988) pp. 181–93.
5. *Ceram. Source, Amer. Ceram. Soc.* **3** (1987) 229.
6. N. R. ADSIT, in "Compression testing of Homogeneous Materials and Composites", ASTM STP 808, edited by R. Chait and R. Papirno (American Society for Testing and Materials, Philadelphia, PA, 1983) pp. 175–86.
7. R. J. LEE, *Composites* **18** (1987) 35.
8. J. LANKFORD, *J. Mater. Sci.* **11** (1978) 351.
9. *Idem, ibid.* **16** (1981) 1567.
10. B. D. LAUTERWASSER and E. J. KRAMER, Materials Science Center Report 3076, Cornell University, August 1978.
11. H. T. HAHN and J. G. WILLIAMS, in "Composite Materials: Testing and Design" (Seventh Conference), ASTM STP 893, edited by J. M. Whitney (American Society for Testing and Materials, Philadelphia, PA, 1986) pp. 115–39.
12. J. LANKFORD, *Mater. Sci. Engng* **A107** (1989) 261.

Received 27 April
and accepted 2 June 1992